OPAL Physics Note PN 299
25th July 1997

Identified Charged Particle Production in Quark and Gluon Jets

The OPAL Collaboration

Abstract

The production rates of $e^{\pm}$, $\pi^{\pm}$, $K^{\pm}$, and $p(\bar{p})$ from hadronic Z^0 decays have been determined with the OPAL detector at LEP using the measurements of the specific energy loss dE/dx of particles in a data sample of about 1.7 million events. The inclusive particle rates per event have been found to be 0.41 ± 0.12 for electrons, 17.10 ± 0.18 for pions, 2.33 ± 0.09 for kaons, and 1.04 ± 0.10 for protons. The inclusive particle momentum spectra and total rates are compared with the predictions of different Monte Carlo models and the measurements of other LEP experiments. In addition charged particle production has been studied in quark and gluon jets in 3-jet events selected with the Durham jet finder with a cut off value of $y_{\rm cut} = 0.005$. The jets are classified on a statistical basis as quark or gluon induced jets according to their energy. Relative production rates, defined as the specific particle production rate divided by the charged multiplicity, have been obtained in quark and gluon jets. The ratios of these relative production rates in gluon and quark jets have been determined to be 1.02 ± 0.01 for pions, 0.95 ± 0.03 for kaons, and 1.10 ± 0.04 for protons.

This note describes preliminary OPAL results to be submitted to the XVIII International Symposium on Lepton-Photon Interactions, Hamburg, 28 July - 1 August 1997, and to the International Europhysics Conference on High Energy Physics, Jerusalem, 19-26 August 1997.

1 Introduction

The production rates of identified charged particles in e^+e^- annihilations are an important input to fragmentation models [1, 2]. Whereas inclusive and differential rates have been measured at the Z^0 peak by most of the LEP collaborations [3–5] and by several experiments at lower energies around $\sqrt{s} = 10\,\mathrm{GeV}$ [6, 7] and at $\sqrt{s} = 29\,\mathrm{GeV}$ [8–11], rather little information is available on particle production in quark and gluon jets. Charged particle multiplicities in jets have been measured previously in onefold or threefold symmetric 3-jet events [12, 13], facilitating the comparison between quark and gluon jets of equal energies. The production of identified particles in jets has been studied in two recent publications [14, 15].

In this paper the inclusive production of charged particles is investigated using measurements of their specific energy loss, $\mathrm{d}E/\mathrm{d}x$, in bins of the particle momentum. The $\mathrm{d}E/\mathrm{d}x$ measurement allows particle identification over a large momentum range with the exception of the region between approximately 1–3 GeV/c where the identification is ambiguous due to overlapping $\mathrm{d}E/\mathrm{d}x$ distributions. Below 1 GeV/c the $\mathrm{d}E/\mathrm{d}x$ distributions of the individual particle species are well separated such that the identification is possible on a track-by-track basis. Above 3 GeV/c only a statistical separation of the different particle species is possible, and in each momentum bin the particle multiplicities are determined from a maximum likelihood fit to the experimental data. The results on inclusive charged particle production presented in this paper supersede an earlier OPAL work [3].

In a recent paper of the OPAL collaboration [16] the production of K^0_S and Λ in quark and gluon jets has been investigated. The present paper contains the extension of this analysis to the charged particles $\pi^\pm$, $K^\pm$, and $p(\bar{p})$. 3-jet events are selected using the Durham jet finder with a cut off value of $y_{\mathrm{cut}} = 0.005$. The jets are classified as quark or gluon induced jets on a statistical basis according to their energy. Gluon jets are expected to have on average the smallest energy. The energy dependence of the gluon jet purity is determined from Monte Carlo models. The different energy ranges of quark and gluon jets are accounted for by comparing relative rates in bins of the jet energy. These relative rates are defined as the ratio of the specific particle production rate and the charged multiplicity in each jet energy bin. They are assumed to be independent of the jet energy for pure quark and gluon jet samples.

The paper is organized as follows: in section 2 the OPAL detector and the $\mathrm{d}E/\mathrm{d}x$ measurement are described, followed by a discussion of the selection of events and tracks. In section 3 the maximum likelihood procedure used to measure the particle rates is presented. Inclusive charged particle production in the total event sample is discussed in section 4, and particle production in 3-jet events is investigated in section 5. A summary is given in section 6.

2 The OPAL Detector and Data Sample

2.1 The OPAL Detector

The OPAL detector at LEP is a multipurpose detector and has been described in detail elsewhere [17]. In the following only the detector elements relevant for this analysis, namely the central tracking chambers and the electromagnetic calorimeters, are described in some detail.

The central detector consists of a silicon microvertex detector [18] and three drift chamber devices, the vertex detector, a large jet chamber, and surrounding z-chambers. The silicon microvertex detector is closest to the beam pipe. It consists of two layers of silicon strips with a single hit resolution of about 10 μm in the $r\phi$ plane.[1] The vertex chamber is a cylindrical drift chamber with an inner layer of 36 cells each containing 12 sense wires, and an outer layer of 36 stereo cells each with 6 sense wires. It covers a range of $|\cos\theta| < 0.95$. Its single hit resolution is 50 μm in the $r\phi$ plane and 700 μm in the z direction. Most important for this analysis is the jet chamber. It is a cylindrical drift chamber with an inner radius of 25 cm, an outer radius of 185 cm, and a length of about 4 m. The chamber is subdivided into 24 sectors in ϕ, each equipped with 159 sense wires spaced by 1 cm. The spatial resolution is about 135 μm in the $r\phi$ plane from drift time information and about 6 cm in the z direction from charge division. The z-chambers, each equipped with six wires perpendicular to the beam axis, provide a more accurate z measurement with a resolution of about 300 μm. In combination the three drift chambers yield a momentum resolution of $\sigma_{p_t}/p_t \approx \sqrt{0.02^2 + (0.0015 \cdot p_t)^2}$ for $|\cos(\theta)| < 0.7$, where p_t is the transverse momentum in GeV/c. The first term arises from multiple coulomb scattering [19]. The tracking chambers are surrounded by a solenoid which provides a uniform magnetic field of 0.435 Tesla parallel to the beam direction.

Electromagnetic energy is measured by lead glass calorimeters surrounding the solenoid. They consist of a barrel and two endcap arrays with a total of 11704 lead glass blocks covering a range of $|\cos\theta| < 0.98$. Finally, the whole detector is surrounded by muon chambers.

2.2 dE/dx Measurement

The energy loss of charged particles in matter as described by the Bethe-Bloch equation [20] is a universal function of $\beta\gamma = p/m$ for all particle masses. As a function of the momentum alone it splits into separated curves for the various particle species. Thus, charged particles can be identified by the simultaneous measurement of their specific energy loss, dE/dx, and of their momentum p.

For each charged particle traversing the OPAL jet chamber up to 159 space points and charge deposition measurements are available. The raw charge measurements are subject to quality cuts and corrections [19]. The accepted charge measurements (dE/dx hits) follow a Landau distribution exhibiting a large tail at high dE/dx values. The dE/dx measurement of a track is determined as the truncated mean of this distribution, discarding the upper 30% of the dE/dx hits. The dE/dx resolution obtained with the OPAL jet chamber for 159 dE/dx hits is about 3.1% for isolated tracks and about 3.8% for tracks in a multihadronic environment [19].

Figure 1 shows the separation power of the dE/dx measurement for the different particle species. The separation of two particle species i and j at a given momentum is defined as:

$$\text{Separation} = \frac{|(\mathrm{d}E/\mathrm{d}x)_i - (\mathrm{d}E/\mathrm{d}x)_j|}{\sqrt{\sigma^2_{(\mathrm{d}E/\mathrm{d}x)_i} + \sigma^2_{(\mathrm{d}E/\mathrm{d}x)_j}}}, \tag{1}$$

where $(\mathrm{d}E/\mathrm{d}x)_{i,j}$ and $\sigma_{(\mathrm{d}E/\mathrm{d}x)_{i,j}}$ are the dE/dx measurements of the two particles and their experimental errors. At momenta between approximately 1 and 3 GeV/c, the dE/dx curves of different particle species cross one another, resulting in low separation power in slightly different ranges for the different species. The separation between pions and muons is insufficient to measure the rates of both particles separately. Only the combined rate of pions and muons can

[1]The OPAL coordinate system is defined with the positive z axis along the electron beam direction. r is the coordinate normal to the beam axis, θ and ϕ are the polar and the azimuthal angles.

be measured[2], and the small muon background has to be subtracted.

2.3 Event and Track Selection

The data sample used in this analysis corresponds to 1.7 million hadronic events collected in 1994 with the OPAL detector at the Z^0 peak. Hadronic events have been selected using the standard OPAL multihadron selection [21]. The estimated backgrounds from $e^+e^- \to \tau^+\tau^-$ and two photon events are found to be less than 0.1% and 0.5%, respectively.

To obtain events mostly contained in the sensitive detector volume a number of additional selection criteria have been applied. Events have been retained if they satisfied $|\cos\theta_{\mathrm{thrust}}| < 0.87$ where θ_{thrust} is the thrust vector polar angle defined relative to the beam direction. Charged tracks have been considered if they had more than 25% of the geometrically possible jet chamber hits and at least 20 hits. This corresponds to $|\cos\theta| < 0.94$. The transverse momentum had to exceed a minimum $p_t > 150\,\mathrm{MeV}/c$. The tracks have been required to point to the interaction vertex to within 5 cm in the $r\phi$ plane and 50 cm in z direction. These latter cuts reduce the number of tracks from nuclear interactions while retaining most of the tracks from decays of short lived particles. In order to obtain an acceptable $\mathrm{d}E/\mathrm{d}x$ measurement with the truncated mean method each track has been required to have at least 20 $\mathrm{d}E/\mathrm{d}x$ hits. After these cuts 1 489 102 events with a total of 16 099 696 tracks remain for the analysis of the inclusive production rates. The sample is large enough that the analysis is completely dominated by systematic uncertainties.

Monte Carlo events have been used to correct for detection efficiencies, to check the quality of the experimental procedures, and to compare the results with model predictions. For this purpose 1.7 million JETSET 7.4 [1] events, processed with the OPAL detector simulation package [22], have been used. In addition, 2 million JETSET 7.4 and 2 million HERWIG 5.9 [2] events have been generated for comparisons with model predictions. Both generators have been tuned to agree with the overall event shapes as measured by OPAL. The parameters for the JETSET 7.4 model are given in [23]. The parameters used for HERWIG 5.9 are the same as those given in [23] for HERWIG, version 5.8, except that the value of the cluster mass cutoff `CLMAX` has been increased from 3.40 to 3.75 to improve the model's description of the charged multiplicity in inclusive hadronic Z^0 decays. In addition the parameter `QCDLAM` has been decreased from 0.16 to 0.15, and the gluon effective mass (`RMASS(13)`) has been decreased from 0.75 to 0.70.

3 Charged Particle Identification

The separation of the different charged particle species has been done with an extended maximum likelihood procedure in bins of the particle momentum. The particle rates $\vec{a} = (a_\pi, a_{\mathrm{K}}, a_{\mathrm{p}}, a_{\mathrm{e}})$ are the free parameters of the likelihood function $\mathcal{L}$. They are obtained by minimizing the negative logarithm of the likelihood function:

[2] In the following, the pion rate is understood as the combined rate of pions and muons unless stated differently.

$$
\begin{aligned}
&-\ln \mathcal{L}\left((\mathrm{d}E/\mathrm{d}x)_1, \ldots, (\mathrm{d}E/\mathrm{d}x)_N ; \vec{a}\right) = \\
&\quad -\sum_{i=1}^{N} \ln\left[\sum_{j=\pi,\mathrm{K},\mathrm{p},\mathrm{e}} a_j P_j\left((\mathrm{d}E/\mathrm{d}x)_i ; \mu_j(p_i), \sigma_j, \vec{\alpha}\right)\right] + \sum_{j=\pi,\mathrm{K},\mathrm{p},\mathrm{e}} a_j.
\end{aligned} \tag{2}
$$

Here N is the number of observed tracks, and P_j is the probability to obtain the measurement $(\mathrm{d}E/\mathrm{d}x)_i$ under the particle hypothesis j, with $\mu_j(p_i)$ and σ_j being the expected mean and width of the distribution for the hypothesis j. The second term $\sum_{j=\pi,\mathrm{K},\mathrm{p},\mathrm{e}} a_j$ is the total number of expected tracks. The probability distributions P_j are approximated by Gaussian functions with additional small tails to account for experimental effects which are described by a parameter vector $\vec{\alpha} = (\alpha_1, \alpha_2, \alpha_3)$. The mean $\mu_j(p_i)$ is the expected energy loss, calculated from the Bethe-Bloch equation, of track i with momentum p_i for the particle hypothesis j. The width σ_j is the expected experimental error which is determined from the experimental error $\sigma_{(\mathrm{d}E/\mathrm{d}x)_i}$ and the measured energy loss $(\mathrm{d}E/\mathrm{d}x)_i$ of track i [19]:

$$
\sigma_j = \frac{\sigma_{(\mathrm{d}E/\mathrm{d}x)_i}}{(\mathrm{d}E/\mathrm{d}x)_i} \mu_j(p_i). \tag{3}
$$

3.1 Parametrization of dE/dx Distributions

The application of the maximum likelihood procedure requires a proper parametrization of the probability distributions $P_j\left((\mathrm{d}E/\mathrm{d}x)_i ; \mu_j(p_i), \sigma_j, \vec{\alpha}\right)$ including the non-Gaussian tails. The tails are parametrized by adding a Breit-Wigner-like term to the ideal Gaussian distribution. Thus, the probability distribution P_j can be written as:

$$
\begin{aligned}
P_j((\mathrm{d}E/\mathrm{d}x)_i; \mu_j(p_i), \sigma_j, \vec{\alpha}) \;=\; & \frac{1}{1+\alpha_1} \cdot \left\{ \frac{1}{\sqrt{2\pi}\sigma_j} \exp\left(-\frac{1}{2}\left(\frac{(\mathrm{d}E/\mathrm{d}x)_i - \mu_j(p_i)}{\sigma_j}\right)^2\right) \right. \\
& \left. + \frac{\alpha_1}{\pi} \cdot \frac{\sigma_j \alpha_3/2}{\left((\mathrm{d}E/\mathrm{d}x)_i - \mu_j(p_i) - \sigma_j\alpha_2\right)^2 + (\sigma_j\alpha_3/2)^2} \right\},
\end{aligned} \tag{4}
$$

where the three parameters $\vec{\alpha} = (\alpha_1, \alpha_2, \alpha_3)$ determine the relative amount and the shape of the additional Breit-Wigner term, σ_j is the expected $\mathrm{d}E/\mathrm{d}x$ resolution according to equation (3), and $\mu_j(p_i)$ is the expected mean as defined in the previous section. In the most general case the resolution and the tail parameters might also depend on the momentum p_i of the track.

This parametrization of the probability distributions $P_j\left((\mathrm{d}E/\mathrm{d}x)_i ; \mu_j(p_i), \sigma_j, \vec{\alpha}\right)$ has been obtained from distributions of the normalized $\mathrm{d}E/\mathrm{d}x$ which is defined as

$$
(\mathrm{d}E/\mathrm{d}x)_{\mathrm{norm},i} = \frac{(\mathrm{d}E/\mathrm{d}x)_i - \mu_j(p_i)}{\sigma_j}, \tag{5}
$$

where $(\mathrm{d}E/\mathrm{d}x)_i$ is the measured $\mathrm{d}E/\mathrm{d}x$ of track i. The shape of the $(\mathrm{d}E/\mathrm{d}x)_{\mathrm{norm}}$ distributions should not depend on the particle species. In an ideal case $(\mathrm{d}E/\mathrm{d}x)_{\mathrm{norm}}$ is expected to follow a Gaussian distribution with a mean of zero and a standard deviation of unity if track i corresponds to the particle hypothesis j.

The $(\mathrm{d}E/\mathrm{d}x)_{\mathrm{norm}}$ distributions have been investigated with $\pi^{\pm}$ from $\mathrm{K}^0_{\mathrm{S}}$ decays which have been selected as described in [26]. The selected $\mathrm{K}^0_{\mathrm{S}}$ sample has a background of less than 10% which is mainly combinatorial resulting in a pion sample with a purity of about 95%.

Figure 2 shows $(\mathrm{d}E/\mathrm{d}x)_{\mathrm{norm}}$ distributions for simulated events and for data in a particular momentum bin. They follow the expected normalized Gaussian over two orders of magnitude. However, a non-Gaussian tail towards high $\mathrm{d}E/\mathrm{d}x$ values of the order of 10^{-2} of the height of the distribution is observed. This tail arises from the limited double track resolution of the jet chamber [19]. Two close-by tracks might be reconstructed as a single track which fakes too large a $\mathrm{d}E/\mathrm{d}x$ measurement. The distribution for experimental data shows an additional small tail at low $\mathrm{d}E/\mathrm{d}x$ values which originates from detector effects in dense tracking environments and is not simulated in the Monte Carlo. The parameters $\vec{\alpha} = (\alpha_1, \alpha_2, \alpha_3)$ have been derived from binned maximum likelihood fits to the $(\mathrm{d}E/\mathrm{d}x)_{\mathrm{norm}}$ distributions. The fit function used is the same as shown in equation (4) for the P_j, except it is expressed in terms of $(\mathrm{d}E/\mathrm{d}x)_{\mathrm{norm}}$. In this case the mean μ_j is expected to be zero and the resolution σ_j should be one, independent of the particle species and the momentum. The latter assumption has been checked by repeating the fits in bins of the momentum, and no significant dependence has been found. The assumption that the $(\mathrm{d}E/\mathrm{d}x)_{\mathrm{norm}}$ distribution is independent of the particle species has been checked by repeating the analysis with identified protons from Λ decays. Again the same parameter values were found within errors for the mean, the resolution and the tail parameters $\vec{\alpha}$.

In table 1 the parameter values for the tail parametrization are shown for data and Monte Carlo simulation. The difference between the value of α_2 in data and simulation stems from different mean values as can be seen from figure 2: the Breit-Wigner function for the data also describes the additional tail at low $\mathrm{d}E/\mathrm{d}x$ values of the experimental data resulting in a shift towards a lower mean. In general, the measurements of the particle production rates depend only weakly on the tail parametrization. The only exception is the electron rate, which, for momenta above $2\,\mathrm{GeV}/c$, is rather sensitive to the parametrization of the positive tail of the pion probability function P_π. For the final fit the measured tail parameters $\vec{\alpha}$ are used in the probability functions P_j for all four particle hypotheses. Figure 3 shows a $\mathrm{d}E/\mathrm{d}x$ distribution in typical momentum bin with the results of the maximum likelihood fit superimposed. Also shown are the probability distributions for the individual particle species.

Parameter	Monte Carlo	Data
α_1 (amount)	0.056 ± 0.002	0.102 ± 0.007
α_2 (mean)	1.84 ± 0.02	0.37 ± 0.06
α_3 (sigma)	1.30 ± 0.02	1.14 ± 0.07

Table 1: Values of the parameters that determine the additional Breit-Wigner term from simulated and experimental events.

4 Measurement of Production Rates

4.1 General Procedure

The production rates of charged pions, kaons, protons, and electrons have been measured as a function of the particle momentum using the maximum likelihood procedure described above. The particle production rates have been measured between 0.15 and $45.0\,\mathrm{GeV}/c$, with the exception of the region between approximately 1.0 and 3.0 GeV/c. In this cross-over region the measurement of particle rates via $\mathrm{d}E/\mathrm{d}x$ is ambiguous. The exact values for the boundaries of the cross-over region can be seen from figures 4–7 and from tables 8–11. For momenta below $0.15\,\mathrm{GeV}/c$ an extrapolation using the JETSET 7.4 Monte Carlo prediction has been applied to all particle rates.

In the cross-over region the production rates can not be measured. Instead an interpolation has been used based on orthogonal Chebyshev polynomials. Polynomials of fourth order are used for the electrons, of sixth order for the kaons, and of eighth order for pions and protons taking into account slight differences in the shape of the fragmentation functions. This interpolation procedure has been checked using Monte Carlo events where it has been verified that the interpolation functions describe the shape of the momentum spectra in the cross-over region. In addition, the fit function provides an excellent description of the data for momenta between 0.15–$1.0\,\mathrm{GeV}/c$ and 3.0–$45.0\,\mathrm{GeV}/c$. The total rates, therefore, have been measured by integrating the fit functions over the momentum range from 0.15–$45.0\,\mathrm{GeV}/c$ and by extrapolating to $0\,\mathrm{GeV}/c$ using the Monte Carlo prediction.

Figures 4–7 show the measured spectra as a function of the momentum, with the fit superimposed. Integrating the fits and extrapolating to all momenta the total production rates per event have been found to be: 0.4102 ± 0.0005 for electrons, 17.10 ± 0.02 for pions, 2.329 ± 0.003 for kaons, and 1.039 ± 0.003 for protons where the errors given are statistical. These total rates include a number of corrections which are discussed in the next section.

4.2 Efficiencies and other Corrections

The results of the maximum likelihood fit have been corrected for efficiency and detector effects in each momentum bin. The efficiencies have been derived from Monte Carlo events for each particle species separately. In addition, the following corrections have been applied:

- All particle rates contain some contributions of tracks from nuclear interactions. These contributions are subtracted using Monte Carlo information. The correction is of the order of 10% for pions. The errors of these corrections are calculated assuming that the detector simulation over- or underestimates the number of tracks from nuclear interactions by at most 20% [3].

- In the momentum region from 0.15–$1.0\,\mathrm{GeV}/c$ only tracks of negatively charged particles are used for the maximum likelihood procedure. They are less affected by nuclear interactions, and are described better by the detector simulation. This reduces the level of necessary corrections. The rates in this momentum region have been doubled in order to account also for positively charged particles.

- The measured $\pi^\pm$ rates have been corrected for the small $\mu^\pm$ background. The correction is smaller than 5% over the whole momentum range. It has been derived from Monte Carlo events. The error of this correction has been calculated assuming that the Monte Carlo simulation describes the $\mu^\pm$ rate to better than $\pm 10\%$ [3]. The use of the muon chambers is not meaningful for this correction because low momentum muons do not reach the chambers.

- The measured $\mathrm{p}(\bar{\mathrm{p}})$ rates have been corrected for hyperon background ($\Sigma^\pm$). As in the case of the $\mu^\pm$ background, the correction factor has been derived from Monte Carlo events. The correction is of the order of 2% for momenta above $20\,\mathrm{GeV}/c$ and is negligible for smaller momenta. The error of the correction is calculated assuming that the JETSET 7.4 model describes the $\Sigma^\pm$ rates to better than $\pm 28\%$ [27].

- The impact of the track selection cuts (see section 2.3) is slightly different in simulated and experimental events. Therefore, the correction factors for the experimental data have been modified with the ratio of the fraction of tracks that pass the cuts in simulated and experimental events, respectively. The correction is smaller than 1% over the whole momentum range.

- Charged particles show a small energy loss in the material in front of the jet chamber. Therefore, the $\mathrm{d}E/\mathrm{d}x$ and momentum measurement in the jet chamber are slightly altered compared to the momentum at the track origin. This effect has been corrected for by shifting the momenta of each particle species accordingly [3]. The shift is between 5% for low momenta and 0.1% for high momenta.

- The electron rate contains a large contribution from photon conversions. This fraction has been determined with simulated events assuming that the rate of gamma rays in the event simulation is known with an error of $\pm 5\%$ [28] and that the detector simulation describes the conversion rate to better than $\pm 5\%$. The amount of conversions can be as large as 80% of the measured rate for momenta around 1 GeV/c.

4.3 Systematic Uncertainties

In each momentum bin the systematic uncertainties of the maximum likelihood fitting procedure and the uncertainties of the various correction factors have been considered. These uncertainties have been propagated to the systematic errors of the integrated rates by the procedure described below. In addition, uncertainties of the integration procedure have been investigated to determine the systematic error of the total rates.

Sources of systematic error of the maximum likelihood procedure are:

- the parametrization of the Bethe-Bloch equation (μ_j);

- the $\mathrm{d}E/\mathrm{d}x$ resolution (σ_j);

- the parametrization of the non-Gaussian tails (α_1, α_2, α_3).

All three sources of systematic errors have been investigated with $(\mathrm{d}E/\mathrm{d}x)_{\mathrm{norm}}$ distributions of $\pi^\pm$ from K^0_S decays as a function of pion momentum both for simulated and experimental events. The parametrization of the Bethe-Bloch equation and the $\mathrm{d}E/\mathrm{d}x$ resolution can be checked by studying the deviations of the mean and standard deviation of the Gaussian part of equation (4) from zero and one, respectively. A correction has been applied to the values of μ_j and σ_j such that the mean and standard deviation of the Gaussian part of equation (4) become zero and one. The variation of μ_j and σ_j is on average 10% and 3% of σ_j, respectively. With these corrected values for μ_j and σ_j the maximum likelihood fit has been repeated. The differences with respect to the standard analysis have been taken as a systematic error.

The systematic errors arising from the parametrization of the non-Gaussian tails have been determined by varying the parameters α_1, α_2 and α_3. The parameters have been shifted simultaneously and separately by $\pm 1\sigma$ of the errors from the fits of equation (4) to the $(\mathrm{d}E/\mathrm{d}x)_{\mathrm{norm}}$ distributions in order to take correlations of the parameters α_1, α_2, and α_3 into account in the appropriate way.

Table 2 gives a summary of the systematic uncertainties of the maximum likelihood procedure. As these uncertainties are almost independent of the momentum, only the average values are shown. The dominant systematic errors arise from the parametrization of the Bethe-Bloch equation (μ_j). The influence of the $\mathrm{d}E/\mathrm{d}x$ resolution (σ_j) is almost negligible. The parametrization of the non-Gaussian tails (α_1, α_2, α_3) yields a significant contribution to the total systematic error only for electrons. Again, these results do not depend significantly on the particle momentum. Therefore, they have been assumed to be fully correlated in momentum.

Source of systematic error	Monte Carlo				Data			
	$e^{\pm}$ [%]	$\pi^{\pm}$ [%]	$K^{\pm}$ [%]	$p(\bar{p})$ [%]	$e^{\pm}$ [%]	$\pi^{\pm}$ [%]	$K^{\pm}$ [%]	$p(\bar{p})$ [%]
μ_j	10	0.5	2	6	5	0.7	2.6	10
σ_j	5	0.1	1	1	<0.01	<0.01	<0.01	<0.01
α_1, α_2, α_3	1	0.1	0.5	0.5	3.6	0.05	0.4	0.05
Sum	11.2	0.52	2.3	6.1	6.2	0.70	2.6	10.0

Table 2: Systematic errors in percent for the individual particle rate measurements associated with the maximum likelihood procedure. For the sum of the systematic errors the single contributions have been added in quadrature. The numbers given are averaged over the whole momentum range.

The errors of the total rates are summarized in table 3 They have been obtained in the following way: the statistical errors from the maximum likelihood fit and the errors of the various corrections factors have been added in quadrature in each momentum bin assuming no correlation. The systematic errors of the maximum likelihood fit have been considered separately because they are fully correlated in momentum.

The interpolation fits using Chebyshev polynomials have been performed using the uncorrelated errors first. Then the interpolation functions have been integrated in order to yield the total rates in the momentum region 0.15–45.0 GeV/c. In a second step, the fully correlated errors of the maximum likelihood procedure have been taken into account by the following procedure. The measured points were shifted by $\pm 1\sigma$ of the fully correlated systematic errors. With these shifted points the integration was repeated. This yielded two new interpolation functions: one representing the lower limit of the total rate and the other the upper limit (see shaded bands in figures 4–7). The largest deviation of the new rates from the standard measurements has been included in the systematic error of the total rate.

For momenta below 0.15 GeV/c the extrapolated fraction of the rate predicted by the JETSET 7.4 model has been added. The difference of the JETSET 7.4 and HERWIG 5.9 predictions has been taken as the error of the extrapolated rate.

In addition, possible uncertainties of the shape of the interpolation function have been considered. For that purpose, the determination of the particle rates has been repeated with Monte Carlo events. The resulting rates have been compared to the generated rates and the difference has been added in quadrature to the systematic error of the total rates.

Finally, the statistical error of the total rates is obtained from the quadratic sum of the statistical errors in each momentum bin.

Table 3 gives an overview of the total rates and the different contributions to the systematic errors. In tables 8–11 the differential rates in each momentum bin are listed together with their statistical and systematic errors.

	$e^{\pm}$	$\pi^{\pm}$	$K^{\pm}$	$p(\bar{p})$
Rate				
Integration, $p > 0.15\,\mathrm{GeV}/c$	0.3007	16.69	2.324	1.038
Extrapolation, $p < 0.15\,\mathrm{GeV}/c$	0.1095	0.41	0.005	0.001
Systematic errors				
Integration	±0.1175	±0.12	±0.061	±0.104
Extrapolation	±0.0008	±0.01	±0.001	±0.0001
Shape	±0.0203	±0.13	±0.069	±0.006
Total rates with errors				
Total rate	0.4102	17.10	2.329	1.039
Stat. error	±0.0005	±0.02	±0.003	±0.003
Total sys. error	±0.1192	±0.18	±0.092	±0.104

Table 3: Total rates per event and errors for the different particle species.

The dominant systematic error depends on the particle species. For the pion rate it arises from the 10% uncertainty of the muon-correction which results in a 0.5% error on the total pion rate compared to the total error of the order of 1%. The largest contribution to the total error of the kaon rate arises from the interpolation because kaons have the largest cross-over region. This leads to larger uncertainties of the interpolation compared to the other particle species. For protons and electrons all sources of systematic error contribute approximately equally. The systematic errors dominate the total error for all particle species.

4.4 Discussion and Comparisions with other LEP Experiments

Table 4 gives a comparison of the final results with the earlier OPAL [3] and the DELPHI [5] measurements[3] as well as with the predictions of the JETSET 7.4 and HERWIG 5.9 models.[4] All comparisons with model predictions refer to the OPAL tuned versions as described in section 2.3. Compared to the previous OPAL results a higher accuracy has been achieved due to improved modelling of the $\mathrm{d}E/\mathrm{d}x$ distributions, in addition to the larger event sample. The total pion rate is in agreement with the previous OPAL measurement. Both the total kaon and the total proton rate are consistent with the earlier OPAL measurements and with the results from DELPHI. The momentum spectra also agree well with the earlier OPAL measurements and the DELPHI and ALEPH [4] results. The proton rate at high momenta has slightly increased compared to the previous OPAL measurement and is similar to the results of DELPHI and ALEPH. Finally, for the first time a measurement of the inclusive electron rate has been possible.

In figures 4–7 the JETSET 7.4 and HERWIG 5.9 Monte Carlo predictions are compared to the measurements of the particle spectra. The Monte Carlo rates have been normalized to the data to make a comparison of the shape of the spectra reasonable. The scaling factor is the weighted average of the ratios of Monte Carlo and data in each momentum bin. In general, the

[3] ALEPH [4] published only differential rates.

[4] In the Monte Carlo samples all particles with a mean lifetime smaller than $3 \cdot 10^{-10}$ seconds are forced to decay. Therefore, the pions rates contain contributions from K^0_S decays, but not from K^0_L and $K^{\pm}$ decays. Accordingly the proton rates contain contributions from Λ decays.

	$e^{\pm}$	$\pi^{\pm}$	$K^{\pm}$	$p(\bar{p})$
This analysis	0.41 ± 0.12	17.10 ± 0.18	2.33 ± 0.09	1.04 ± 0.10
OPAL [3]	—	17.05 ± 0.43	2.42 ± 0.13	0.92 ± 0.11
DELPHI [5]	—	—	2.26 ± 0.18	1.07 ± 0.14
JETSET 7.4	0.38	17.61	2.11	0.94
HERWIG 5.9	0.38	17.02	2.18	1.42

Table 4: Comparison of the results of this analysis with the published rates of OPAL and DELPHI as well as with the predictions of the JETSET 7.4 and HERWIG 5.9 Monte Carlo models.

Monte Carlo models describe the measured fragmentation functions and the total rates quite well. Both models, however, predict too soft a kaon spectrum and too hard a proton spectrum.

5 Charged Particle Production in Quark and Gluon Jets

In this section the production rates of identified charged particles, $\pi^{\pm}$, $K^{\pm}$, and $p(\bar{p})$ in quark and gluon jets are compared. The analyis is done in 3-jet events, in which the jets are classified as quark or gluon jets according to their energy. The lowest energy jet is preferentially the gluon jet, the highest energetic one a quark jet. After a discussion on the selection of 3-jet events and the method of identifying quark and gluon jets, particle production in these jets is studied, and sources of systematic uncertainties are investigated. Finally, the results are presented and discussed.

5.1 Selection of 3-jet Events

Jets are reconstructed with the Durham jet finder [24] with a cut-off value of $y_{\rm cut} = 0.005$. This $y_{\rm cut}$ value is the same as used in [16] in a similar analysis. Jets have been reconstructed from charged tracks and electromagnetic clusters. Clusters were considered if they spread over at least 2 lead glass blocks, had an energy greater than 200 MeV and were not associated with a charged track.[5] Each jet was required to contain at least two charged tracks, to have more than 5 GeV of visible energy and to lie in a region of $|\cos\theta_{\rm jet}| < 0.9$ ($\theta_{\rm jet}$ is the jet axis polar angle). The sum of the angles between all three jets had to exceed 358°, and the angle between the two lower energy jets was required to be larger than 30°. With these criteria 356 993 3-jet events were available for further analysis corresponding to about 24% of the data sample used for the inclusive analysis presented in the preceding sections.

Finally, since the directions of jets are generally measured with less bias than the jet energies, massless kinematics were used to assign a calculated jet energy to each jet, based on the measured jet directions [25].

Simulated events were used to determine the purity of jet identification as a function of jet energy. The procedure applied is the same as described in [16]. The purities of the gluon jets, defined as the ratio of the number of true gluon jets over the total number of jets in each energy

[5] A cluster is associated with a charged track if the extrapolated track coordinates at the calorimeter match the position of a cluster in the barrel region to better than 80 mrad in ϕ and 150 mrad in θ, or to better than 50 mrad for both ϕ and θ in the endcap region.

bin, are given in figure 8, where the gluon jet purity is shown over the whole energy range. The purities have been shown to be nearly independent of the fragmentation model. They have also been found to remain nearly unchanged when using 3-jet events with and without detector simulation [16]. The purity varies from about 90% to 10% for jets with energies from 10 GeV to 35 GeV corresponding to almost pure gluon jet samples at low energies and almost exclusively true quark jets at high energies.

5.2 Determination of Particle Rates

In the 3-jet events the production rates n^{π}, n^{K}, and n^{p} and the inclusive rate n^{ch} have been investigated in each of the three jets as a function of the jet energy. The energy range from 5 to 45 GeV has been subdivided into bins of 5 GeV width. The rates have been determined in each energy bin in the same way as presented in the preceding sections. Correspondingly, all sources of systematic errors as discussed previously have been considered, and the various correction factors have been redetermined in each energy bin. In addition, a correction has been applied to account for the additional cuts in selecting 3-jet events.

Figure 9 shows the production rates n^{π}, n^{K}, n^{p}, and n^{ch} as a function of the jet energy, together with the predictions of the JETSET 7.4 and HERWIG 5.9 models. Both models describe the inclusive charged particle rate in jets whereas the agreement with the single particle rates in jets is poor. Large discrepancies are observed for the charged kaon and proton spectra.

As already mentioned, gluon jets are mostly those below 20 GeV, and at energies above 30–35 GeV predominantly quark jets are found. In the intermediate energy region there is a mixture of both jet species. Because of these different energy ranges it is not meaningful to compare the absolute particle production rates n_g^i and n_q^i, $i = \pi, \mathrm{K}, \mathrm{p}$, in gluon and quark jets. Instead, relative particle production rates $R^i(E_{\mathrm{jet}}) = n^i(E_{\mathrm{jet}})/n^{\mathrm{ch}}(E_{\mathrm{jet}})$ are measured in bins of the jet energy. These relative rates are defined as the ratio of a specific particle rate $n^i(E_{\mathrm{jet}})$, $i = \pi, \mathrm{K}, \mathrm{p}$, and the charged multiplicity $n^{\mathrm{ch}}(E_{\mathrm{jet}})$ in each jet energy bin.

From Monte Carlo studies of pure quark and gluon jets, and from measurements of the relative rates of identified $\mathrm{K^0_S}$ and Λ [16] it is reasonable to assume that the relative production rates in true quark or gluon jets do not depend on the jet energy. Under this assumption the energy independent relative production rates in true quark and gluon jets, $R_g^i = n_g^i/n_g^{\mathrm{ch}}$ and $R_q^i = n_q^i/n_q^{\mathrm{ch}}$, can be determined by a fit to the measured relative production rates in the oberved mixture of quark and gluon jets

$$R^i(E_{\mathrm{jet}}) = R_g^i \cdot \rho_g(E_{\mathrm{jet}}) + R_q^i \cdot (1 - \rho_g(E_{\mathrm{jet}})). \tag{6}$$

Here $R^i(E_{\mathrm{jet}})$ is the measured rate of particle i in the bin with energy E_{jet} and $\rho_g(E_{\mathrm{jet}})$ is the corresponding gluon jet purity as discussed in the beginning of this section. In figure 10 the measured relative production rates are shown together with the results of the fits and the predictions of the JETSET 7.4 and HERWIG 5.9 models. The χ^2 per degree of freedom of a combined fit to all three particle spectra using the uncorrelated errors yields a value of 15.1/18, consistent with the assumption of energy-independent relative rates in true gluon and quark jets.

For the comparison of particle production in true gluon and quark jets the ratios of relative rates, $R_g^i/R_q^i = (n_g^i/n_g^{\mathrm{ch}})/(n_q^i/n_q^{\mathrm{ch}})$ are studied. Before discussing these results which are given in table 6, the systematic errors are determined.

5.3 Systematic Errors

The following sources of systematic errors of the ratios R^i_g/R^i_q have been considered, and the differences with respect to the standard analysis have been taken as a contribution to the systematic error:

- The ranges of the fits of equation (6) to the relative rates have been changed. The fits have been repeated dropping either the first or the last jet energy bin.
- The fits to the relative rates have been repeated with the gluon jet purity $\rho_g(E_{\rm jet})$ varied by $\pm 10\%$ (corresponding to a $\pm 2\sigma$ variation) in each jet energy bin.
- In an alternative approach to extract the relative rates in true gluon and quark jets, the relative rates have been taken as a function of the gluon jet purity [16]. A straight line fit then allows one to obtain the relative rates in pure gluon and quark jets by extrapolating to gluon purity 100% and 0%, respectively.
- Possible deviations from the assumption of constant relative rates in pure quark and gluon jets have been taken into account. The fits of equation (6) have been repeated after replacing $R^i_{g,q}$ by $R^i_{g,q} \cdot (1 + s^i_{g,q} \cdot E_{\rm jet})$ where $s^i_{g,q}$ are the slopes of the relative rates in true quark and gluon jets as determined from the JETSET 7.4 and HERWIG 5.9 models. These slopes are of the order of 10^{-3} for all particles.
- Finally, the whole procedure to determine relative production rates of identified charged particles in identified jets has been performed using Monte Carlo events with detector simulation. The difference to the generated Monte Carlo ratios has been included in the systematic error.

Source of sys. error	$\pi^\pm$ [%]	$\mathrm{K}^\pm$ [%]	$\mathrm{p}(\bar{\mathrm{p}})$ [%]
Fit range	$\pm$ 0.39	$\pm$ 2.10	$\pm$ 1.18
ρ_g variation	$\pm$ 0.20	$\pm$ 0.63	$\pm$ 1.00
Fit procedure	$\pm$ 0.10	$\pm$ 0.10	$\pm$ 0.09
Constant relative rates	$\pm$ 0.89	$\pm$ 0.84	$\pm$ 1.73
Monte Carlo Reconstruction	$\pm$ 0.10	$\pm$ 1.80	$\pm$ 0.73
Total sys. error	$\pm$ 1.00	$\pm$ 2.96	$\pm$ 2.43

Table 5: Contributions (in percent) to the systematic errors of the ratios of the relative rates in gluon and quark jets.

In table 5 the contributions to the systematic error are given. For pions and kaons the dominant systematic error arises from the variation of the fit range. For protons the dominant systematic error stems from the assumption of constant relative rates in true quark and gluon jets. The uncertainties from the reconstruction contribute significantly to the systematic error only for the kaons. As mentioned above, this is a consequence of the particularly large momentum gap without particle identification for kaons.

5.4 Results

Table 6 gives the ratios R^i_g/R^i_q of the relative particle production rates in true gluon and quark jets as extracted from the fits shown in figure 10. The errors have been obtained from the propagation of uncorrelated errors because correlated systematic errors in numerator and denominator cancel.

R^i_g/R^i_q	OPAL				
$\pi^\pm$	1.016	$\pm$	0.010	$\pm$	0.010
$K^\pm$	0.948	$\pm$	0.017	$\pm$	0.028
$p(\bar{p})$	1.100	$\pm$	0.024	$\pm$	0.027

Table 6: Ratios of the normalized particle rates R^i_g/R^i_q in gluon and quark jets.

As already concluded from the shape of the $R^i(E_{\rm jet})$ distributions, $\pi^\pm$ and $p(\bar{p})$ production is slightly larger in gluon jets than in quark jets. $K^\pm$, however, are produced a little more frequently in quark jets.

R^i_g/R^i_q	OPAL			JETSET 7.4	HERWIG 5.9	DELPHI [14]		
$\pi^\pm$	1.02	$\pm$	0.01	1.01	1.05		—	
$K^\pm$	0.95	$\pm$	0.03	0.90	0.73	0.93	$\pm$	0.04
K^0_S	1.10	$\pm$	0.03	0.93	0.73	1.13	$\pm$	0.16
$p(\bar{p})$	1.10	$\pm$	0.04	1.38	1.02	1.12	$\pm$	0.12
Λ	1.41	$\pm$	0.06	1.27	0.88	1.40	$\pm$	0.38

Table 7: Summary of experimental results on relative charged and neutral [16] particle rates in gluon and quark jets. Also shown are the predictions of the JETSET 7.4 and HERWIG 5.9 models.

A comparison of the results of this analysis with recent OPAL work on K^0_S and Λ production in jets [16] and with DELPHI measurements using onefold symmetric 3-jet events [14] is given in table 7. Also included are the JETSET 7.4 and HERWIG 5.9 predictions.[6] For all particle species the agreement of the OPAL results with DELPHI is good. However, the errors in the OPAL analyses are significantly smaller. JETSET 7.4 gives ratios R^π_g/R^π_q and R^K_g/R^K_q similar to those from this analysis, but the measured relative rates R^p and R^K are significantly above and below the experimental rates. Compared to charged kaons the ratio of the relative production rates in gluon and quark jets of neutral kaons is significantly larger. The experimental ratio R^p_g/R^p_q is much smaller than the JETSET 7.4 prediction and also than the experimental ratio of the Λ baryon R^Λ_g/R^Λ_q. Naively, one would expect a similar behaviour for neutral and charged kaons and also for Λ baryons and protons as it is basically predicted by JETSET 7.4 and HERWIG 5.9.

[6] The model predictions as given by DELPHI differ considerably from the values shown in table 7, probably due to different parameter tuning.

6 Summary

In this analysis the production of identified charged particles measured in 1.7 million hadronic Z^0 decays with the OPAL detector at the LEP e^+e^- collider has been investigated. Particle identification has been done using the measurements of the specific energy loss, dE/dx, and of the particle momentum.

In the first part of the paper the inclusive production properties of $e^{\pm}$, $\pi^{\pm}$, $K^{\pm}$, and $p(\bar{p})$ have been determined by studying for each particle species the momentum spectra and the total inclusive production rates which have been found to be 0.41 ± 0.12 for electrons, 17.10 ± 0.18 for pions, 2.33 ± 0.09 for kaons, and 1.04 ± 0.10 for protons. Good agreement has been found with earlier measurements by OPAL and the other LEP collaborations. The previous OPAL measurement of the proton spectrum has been improved in the high momentum region. The JETSET 7.4 and the HERWIG 5.9 models are both able to describe the measurements.

In the second part the production of identified charged particles in jets has been studied. Using the Durham algorithm with $y_{\mathrm{cut}} = 0.005$, about 24% of the data have been selected as 3-jet events. In order to compensate for the different energy ranges of (low energy) gluon jets and (high energy) quark jets, particle production in gluon and quark jets in bins of the jet energy has been compared by studying relative rates, the rates normalized to the inclusive charged particle rate in each jet energy bin. The ratios of relative rates in true gluon and quark jets have been found to be 1.02 ± 0.01 for pions, 0.95 ± 0.03 for kaons, and 1.10 ± 0.04 for protons. Pions and protons have been found to be more frequently produced in gluon jets, while charged kaons are produced more often in quark jets. The experimental results have been compared with a DELPHI analysis, an earlier OPAL study on K^0_S and Λ production in jets and also to the predictions of the JETSET 7.4 and HERWIG 5.9 models. The results are consistent with those obtained by DELPHI while both models have difficulties to describe the experimental distributions.

References

[1] T. Sjöstrand, Comp. Phys. Comm. **82** (1994) 74.

[2] G. Marchesini, et al., Comp. Phys. Comm. **67** (1992) 465.

[3] OPAL Collaboration, R. Akers et al., Zeit. f. Physik **C 63** (1994) 181.

[4] ALEPH Collaboration, Zeit. f. Physik **C 66** (1995) 355.

[5] DELPHI Collaboration, P. Abreu et al., Nucl. Phys. **B 444** (1995) 3.

[6] CLEO Collaboration, S. Behrends et al., Phys. Rev. **D 31** (1985) 2161.

[7] ARGUS Collaboration, H. Albrecht et al., Zeit. f. Physik **C 39** (1988) 177.

[8] TASSO Collaboration, M. Althoff et al., Zeit. f. Physik **C 17** (1983) 5.

[9] TPC Collaboration, H. Aihara et al., Phys. Rev. Lett. **52** (1984) 577;
TPC Collaboration, H. Aihara et al., Phys. Rev. Lett. **61** (1988) 1263.

[10] Mark II Collaboration, H. Schellman et al., Phys. Rev. **D 31** (1985) 3013.

[11] HRS Collaboration, M. Derrick et al., Phys. Rev. **D 35** (1987) 2639.

[12] OPAL Collaboration, R. Akers et al., Zeit. f. Physik **C 68** (1995) 179.

[13] L3 Collaboration, M. Acciarri et al., Phys. Lett. **B 345** (1995) 74;
ALEPH Collaboration, D. Buskulic et al., Phys. Lett. **B 346** (1995) 389;
DELPHI Collaboration, P. Abreu et al., Zeit. f. Physik **C 70** (1996) 179;
ALEPH Collaboration, D. Buskulic et al., Phys. Lett. **B 384** (1996) 353.

[14] DELPHI Collaboration, P. Abreu et al., CERN-PPE/96-193, submitted to Phys. Lett. **B**.

[15] L3 Collaboration, M. Acciarri et al., CERN-PPE/97-50, submitted to Phys. Lett. **B**.

[16] OPAL Collaboration, Λ *and* $\mathrm{K^0_S}$ *Production in Quark and Gluon Jets Classified by Energy-Ordering*, OPAL Physics Note PN 236.

[17] OPAL Collaboration, Nucl. Instr. and Meth. **A 305** (1991) 275.

[18] P. Allport et al., Nucl. Instr. and Meth. **A 324** (1993) 34;
P. Allport et al., Nucl. Instr. and Meth. **A 346** (1994) 476.

[19] M. Hauschild et. al., Nucl. Instr. and Meth. **A 314** (1992) 74.

[20] H. A. Bethe, "Handbuch der Physik" **24/1** (Springer Berlin, 1933) 491.

[21] OPAL Collaboration, G. Alexander et al., Zeit. f. Physik **C 52** (1991) 175.

[22] J. Allison et al., Nucl. Instr. and Meth. **A 317** (1992) 47.

[23] OPAL Collaboration, G. Alexander et al., Zeit. f. Physik **C 69** (1996) 543.

[24] S. Catani, Yu.L. Dokshitzer, F. Fiorani and B.R. Webber, Nucl. Phys. **B 377** (1992) 445; S. Catani et al., Phys. Lett. **B 269** (1991) 432; S. Bethke, Z. Kunszt, D.E. Soper, W.J. Stirling, Nucl. Phys. **B 370** (1992) 310; N. Brown, W.J. Stirling, Zeit. f. Physik **C 53** (1992) 629.

[25] OPAL Collaboration, M.Z. Akrawy et al., Phys. Lett. **B 261** (1991) 334; OPAL Collaboration, G. Alexander et al., Phys. Lett. **B 265** (1991) 462.

[26] OPAL Collaboration, R. Akers et al., Zeit. f. Physik **C 68** (1995) 1.

[27] OPAL Collaboration, G. Alexander et al., Zeit. f. Physik **C 73** (1997) 587.

[28] A. Böhrer, *Inclusive particle production in hadronic decays of the Z boson at LEP I*, preprint CERN-OPEN/96-021, Si-96-15, submitted to Phys. Rep.; I.G. Knowles and G.D. Lafferty, J. Phys. G: Nucl. Part. Phys. 23 (1997), 731.

$\mathrm{e}^{\pm}$							
$p\,[\mathrm{GeV}/c]$	$\frac{1}{\sigma_{\mathrm{had}}}\cdot\frac{\mathrm{d}\sigma}{\mathrm{d}p}$	$\pm\ \Delta_{\mathrm{stat}}$	$\pm\ \Delta_{\mathrm{sys}}$	$p\,[\mathrm{GeV}/c]$	$\frac{1}{\sigma_{\mathrm{had}}}\cdot\frac{\mathrm{d}\sigma}{\mathrm{d}p}$	$\pm\ \Delta_{\mathrm{stat}}$	$\pm\ \Delta_{\mathrm{sys}}$
0.20 – 0.21	0.432	± 0.027	± 0.004	6.69 – 7.21	0.00779	± 0.00048	± 0.00016
0.21 – 0.23	0.344	± 0.021	± 0.003	7.21 – 7.77	0.00681	± 0.00042	± 0.00015
0.23 – 0.25	0.297	± 0.018	± 0.003	7.77 – 8.37	0.00641	± 0.00039	± 0.00015
0.25 – 0.27	0.290	± 0.018	± 0.002	8.37 – 9.03	0.00566	± 0.00035	± 0.00015
0.27 – 0.29	0.255	± 0.016	± 0.002	9.03 – 9.73	0.00502	± 0.00031	± 0.00014
0.29 – 0.31	0.242	± 0.015	± 0.002	9.73 – 10.49	0.00435	± 0.00027	± 0.00013
0.31 – 0.33	0.223	± 0.014	± 0.002	10.49 – 11.30	0.00378	± 0.00023	± 0.00012
0.33 – 0.36	0.204	± 0.013	± 0.001	11.30 – 12.18	0.00332	± 0.00020	± 0.00012
0.36 – 0.39	0.190	± 0.012	± 0.001	12.18 – 13.13	0.00280	± 0.00017	± 0.00011
0.39 – 0.42	0.179	± 0.011	± 0.001	13.13 – 14.15	0.00244	± 0.00015	± 0.00010
0.42 – 0.45	0.162	± 0.010	± 0.001	14.15 – 15.26	0.00225	± 0.00014	± 0.00010
0.45 – 0.48	0.1448	± 0.0089	± 0.0011	15.26 – 16.44	0.00179	± 0.00011	± 0.00009
0.48 – 0.52	0.1319	± 0.0081	± 0.0010	16.44 – 17.73	0.001532	± 0.000094	± 0.000087
2.01 – 2.17	0.0291	± 0.0018	± 0.0004	17.73 – 19.11	0.001200	± 0.000074	± 0.000074
2.17 – 2.34	0.0267	± 0.0016	± 0.0004	19.11 – 20.59	0.000967	± 0.000060	± 0.000069
2.34 – 2.52	0.0246	± 0.0015	± 0.0004				
2.52 – 2.72	0.0237	± 0.0015	± 0.0002				
2.72 – 2.93	0.0217	± 0.0013	± 0.0002				
2.93 – 3.16	0.0206	± 0.0013	± 0.0002				
3.16 – 3.40	0.0186	± 0.0011	± 0.0002				
3.40 – 3.67	0.0168	± 0.0010	± 0.0002				
3.67 – 3.96	0.01612	± 0.00099	± 0.00020				
3.96 – 4.26	0.01503	± 0.00093	± 0.00020				
4.26 – 4.60	0.01367	± 0.00084	± 0.00019				
4.60 – 4.95	0.01282	± 0.00079	± 0.00019				
4.95 – 5.34	0.01129	± 0.00070	± 0.00018				
5.34 – 5.75	0.01097	± 0.00068	± 0.00019				
5.75 – 6.20	0.00954	± 0.00059	± 0.00017				
6.20 – 6.69	0.00866	± 0.00053	± 0.00017				

Table 8: Differential cross sections for electrons.

$\pi^{\pm}$											
$p\,[\mathrm{GeV}/c]$	$\frac{1}{\sigma_{\mathrm{had}}} \cdot \frac{\mathrm{d}\sigma}{\mathrm{d}p}$	$\pm$	Δ_{stat}	$\pm$	Δ_{sys}	$p\,[\mathrm{GeV}/c]$	$\frac{1}{\sigma_{\mathrm{had}}} \cdot \frac{\mathrm{d}\sigma}{\mathrm{d}p}$	$\pm$	Δ_{stat}	$\pm$	Δ_{sys}
0.19 – 0.20	7.517	±	0.053	±	0.207	4.26 – 4.60	0.7515	±	0.0053	±	0.0034
0.20 – 0.22	8.992	±	0.063	±	0.211	4.60 – 4.95	0.6586	±	0.0046	±	0.0031
0.22 – 0.23	9.593	±	0.067	±	0.225	4.95 – 5.34	0.5720	±	0.0040	±	0.0028
0.23 – 0.25	10.049	±	0.071	±	0.226	5.34 – 5.75	0.4914	±	0.0034	±	0.0025
0.25 – 0.27	10.484	±	0.074	±	0.188	5.75 – 6.20	0.4282	±	0.0030	±	0.0023
0.27 – 0.29	10.760	±	0.076	±	0.178	6.20 – 6.69	0.3681	±	0.0026	±	0.0021
0.29 – 0.31	10.831	±	0.076	±	0.170	6.69 – 7.21	0.3137	±	0.0022	±	0.0019
0.31 – 0.34	10.981	±	0.077	±	0.161	7.21 – 7.77	0.2648	±	0.0019	±	0.0017
0.34 – 0.36	10.935	±	0.077	±	0.150	7.77 – 8.37	0.2216	±	0.0016	±	0.0015
0.36 – 0.39	10.826	±	0.076	±	0.140	8.37 – 9.02	0.1874	±	0.0013	±	0.0013
0.39 – 0.42	10.640	±	0.075	±	0.133	9.02 – 9.73	0.1552	±	0.0011	±	0.0011
0.42 – 0.45	10.433	±	0.073	±	0.123	9.73 – 10.48	0.12893	±	0.00090	±	0.00102
0.45 – 0.49	10.101	±	0.071	±	0.113	10.48 – 11.30	0.10561	±	0.00074	±	0.00088
0.49 – 0.53	9.759	±	0.068	±	0.106	11.30 – 12.18	0.08572	±	0.00060	±	0.00076
0.53 – 0.57	9.358	±	0.066	±	0.097	12.18 – 13.13	0.06964	±	0.00049	±	0.00067
0.57 – 0.61	8.906	±	0.063	±	0.090	13.13 – 14.15	0.05450	±	0.00038	±	0.00055
0.61 – 0.66	8.473	±	0.059	±	0.083	14.15 – 15.25	0.04356	±	0.00031	±	0.00048
0.66 – 0.71	7.953	±	0.056	±	0.075	15.25 – 16.44	0.03436	±	0.00024	±	0.00040
0.71 – 0.76	7.502	±	0.053	±	0.071	16.44 – 17.72	0.02635	±	0.00018	±	0.00032
2.02 – 2.17	2.314	±	0.016	±	0.019	17.72 – 19.10	0.02003	±	0.00014	±	0.00026
2.17 – 2.34	2.110	±	0.015	±	0.017	19.10 – 20.58	0.01495	±	0.00010	±	0.00021
2.34 – 2.52	1.912	±	0.013	±	0.016	20.58 – 22.19	0.010809	±	0.000076	±	0.000168
2.52 – 2.72	1.718	±	0.012	±	0.006	22.19 – 23.91	0.007936	±	0.000056	±	0.000133
2.72 – 2.93	1.537	±	0.011	±	0.006	23.91 – 25.78	0.005744	±	0.000040	±	0.000107
2.93 – 3.16	1.3760	±	0.0097	±	0.0053	25.78 – 27.78	0.003897	±	0.000027	±	0.000083
3.16 – 3.41	1.2294	±	0.0086	±	0.0048	27.78 – 29.95	0.002696	±	0.000019	±	0.000064
3.41 – 3.67	1.0933	±	0.0077	±	0.0044	29.95 – 32.28	0.001547	±	0.000011	±	0.000048
3.67 – 3.96	0.9682	±	0.0068	±	0.0040	32.28 – 34.79	0.0009678	±	0.0000068	±	0.0000340
3.96 – 4.26	0.8543	±	0.0060	±	0.0037	34.79 – 37.50	0.0004993	±	0.0000035	±	0.0000235

Table 9: Differential cross sections for pions.

$K^{\pm}$											
$p\,[\mathrm{GeV}/c]$	$\frac{1}{\sigma_{\mathrm{had}}} \cdot \frac{\mathrm{d}\sigma}{\mathrm{d}p}$	$\pm$	Δ_{stat}	$\pm$	Δ_{sys}	$p\,[\mathrm{GeV}/c]$	$\frac{1}{\sigma_{\mathrm{had}}} \cdot \frac{\mathrm{d}\sigma}{\mathrm{d}p}$	$\pm$	Δ_{stat}	$\pm$	Δ_{sys}
0.25 – 0.26	0.2503	±	0.0066	±	0.0346	10.48 – 11.29	0.0450	±	0.0012	±	0.0006
0.26 – 0.27	0.2879	±	0.0076	±	0.0324	11.29 – 12.17	0.0391	±	0.0010	±	0.0005
0.27 – 0.29	0.2923	±	0.0077	±	0.0276	12.17 – 13.12	0.03245	±	0.00085	±	0.00045
0.29 – 0.30	0.3191	±	0.0084	±	0.0264	13.12 – 14.14	0.02679	±	0.00070	±	0.00039
0.30 – 0.32	0.3437	±	0.0090	±	0.0249	14.14 – 15.24	0.02253	±	0.00059	±	0.00035
0.32 – 0.35	0.3598	±	0.0095	±	0.0221	15.24 – 16.43	0.01736	±	0.00046	±	0.00029
0.35 – 0.37	0.411	±	0.011	±	0.023	16.43 – 17.71	0.01384	±	0.00036	±	0.00025
0.37 – 0.40	0.425	±	0.011	±	0.021	17.71 – 19.08	0.01117	±	0.00029	±	0.00022
0.40 – 0.43	0.453	±	0.012	±	0.021	19.08 – 20.57	0.00841	±	0.00022	±	0.00018
0.43 – 0.46	0.490	±	0.013	±	0.020	20.57 – 22.17	0.00649	±	0.00017	±	0.00015
0.46 – 0.49	0.544	±	0.014	±	0.021	22.17 – 23.90	0.00491	±	0.00013	±	0.00013
2.72 – 2.93	0.2846	±	0.0075	±	0.0053	23.90 – 25.76	0.003589	±	0.000094	±	0.000101
2.93 – 3.16	0.2613	±	0.0069	±	0.0036	25.76 – 27.77	0.002527	±	0.000066	±	0.000083
3.16 – 3.40	0.2386	±	0.0063	±	0.0028	27.77 – 29.93	0.001783	±	0.000047	±	0.000065
3.40 – 3.67	0.2205	±	0.0058	±	0.0024	29.93 – 32.26	0.001259	±	0.000033	±	0.000051
3.67 – 3.95	0.2047	±	0.0054	±	0.0021	32.26 – 34.77	0.000775	±	0.000020	±	0.000038
3.95 – 4.26	0.1904	±	0.0050	±	0.0019	34.77 – 37.48	0.000439	±	0.000012	±	0.000026
4.26 – 4.59	0.1760	±	0.0046	±	0.0017	37.48 – 40.40	0.0002414	±	0.0000064	±	0.0000189
4.59 – 4.95	0.1607	±	0.0042	±	0.0016						
4.95 – 5.34	0.1455	±	0.0038	±	0.0014						
5.34 – 5.75	0.1337	±	0.0035	±	0.0013						
5.75 – 6.20	0.1220	±	0.0032	±	0.0012						
6.20 – 6.68	0.1095	±	0.0029	±	0.0011						
6.68 – 7.20	0.1000	±	0.0026	±	0.0010						
7.20 – 7.76	0.0888	±	0.0023	±	0.0009						
7.76 – 8.37	0.0789	±	0.0021	±	0.0008						
8.37 – 9.02	0.0690	±	0.0018	±	0.0008						
9.02 – 9.72	0.0619	±	0.0016	±	0.0007						
9.72 – 10.48	0.0540	±	0.0014	±	0.0006						

Table 10: Differential cross sections for kaons.

p($\bar{\mathrm{p}}$)											
p [GeV/c]	$\frac{1}{\sigma_{\mathrm{had}}} \cdot \frac{\mathrm{d}\sigma}{\mathrm{d}p}$	±	Δ_{stat}	±	Δ_{sys}	p [GeV/c]	$\frac{1}{\sigma_{\mathrm{had}}} \cdot \frac{\mathrm{d}\sigma}{\mathrm{d}p}$	±	Δ_{stat}	±	Δ_{sys}
0.32 – 0.33	0.127	±	0.013	±	0.019	6.68 – 7.20	0.0417	±	0.0042	±	0.0007
0.33 – 0.35	0.146	±	0.015	±	0.021	7.20 – 7.76	0.0369	±	0.0037	±	0.0006
0.35 – 0.36	0.150	±	0.015	±	0.020	7.76 – 8.36	0.0319	±	0.0032	±	0.0005
0.36 – 0.38	0.148	±	0.015	±	0.017	8.36 – 9.01	0.0282	±	0.0028	±	0.0005
0.38 – 0.40	0.149	±	0.015	±	0.014	9.01 – 9.71	0.0233	±	0.0023	±	0.0004
0.40 – 0.42	0.157	±	0.016	±	0.013	9.71 – 10.47	0.0202	±	0.0020	±	0.0004
0.42 – 0.45	0.173	±	0.017	±	0.014	10.47 – 11.29	0.0176	±	0.0018	±	0.0004
0.45 – 0.47	0.182	±	0.018	±	0.013	11.29 – 12.16	0.0156	±	0.0016	±	0.0003
0.47 – 0.51	0.192	±	0.019	±	0.012	12.16 – 13.11	0.0125	±	0.0013	±	0.0003
0.51 – 0.54	0.208	±	0.021	±	0.012	13.11 – 14.13	0.0105	±	0.0010	±	0.0003
0.54 – 0.58	0.214	±	0.021	±	0.011	14.13 – 15.23	0.00853	±	0.00085	±	0.00023
0.58 – 0.62	0.227	±	0.023	±	0.011	15.23 – 16.42	0.00724	±	0.00072	±	0.00021
0.62 – 0.67	0.232	±	0.023	±	0.010	16.42 – 17.69	0.00586	±	0.00059	±	0.00018
0.67 – 0.71	0.249	±	0.025	±	0.010	17.69 – 19.07	0.00438	±	0.00044	±	0.00015
0.71 – 0.77	0.255	±	0.025	±	0.010	19.07 – 20.56	0.00345	±	0.00035	±	0.00013
0.77 – 0.83	0.257	±	0.026	±	0.009	20.56 – 22.16	0.00258	±	0.00026	±	0.00011
0.83 – 0.89	0.270	±	0.027	±	0.009	22.16 – 23.88	0.00185	±	0.00018	±	0.00008
2.72 – 2.93	0.131	±	0.013	±	0.004	23.88 – 25.74	0.00132	±	0.00013	±	0.00007
2.93 – 3.16	0.121	±	0.012	±	0.003	25.74 – 27.74	0.000858	±	0.000086	±	0.000049
3.16 – 3.40	0.117	±	0.012	±	0.002	27.74 – 29.90	0.000537	±	0.000054	±	0.000039
3.40 – 3.67	0.109	±	0.011	±	0.002	29.90 – 32.23	0.000335	±	0.000033	±	0.000029
3.67 – 3.95	0.0961	±	0.0096	±	0.0014	32.23 – 34.74	0.000153	±	0.000015	±	0.000018
3.95 – 4.26	0.0889	±	0.0089	±	0.0013	34.74 – 37.45	0.000101	±	0.000010	±	0.000013
4.26 – 4.59	0.0799	±	0.0080	±	0.0011	37.45 – 40.36	0.0000428	±	0.0000043	±	0.0000072
4.59 – 4.95	0.0717	±	0.0072	±	0.0010						
4.95 – 5.34	0.0657	±	0.0066	±	0.0009						
5.34 – 5.75	0.0589	±	0.0059	±	0.0009						
5.75 – 6.20	0.0526	±	0.0053	±	0.0008						
6.20 – 6.68	0.0459	±	0.0046	±	0.0007						

Table 11: Differential cross sections for protons.

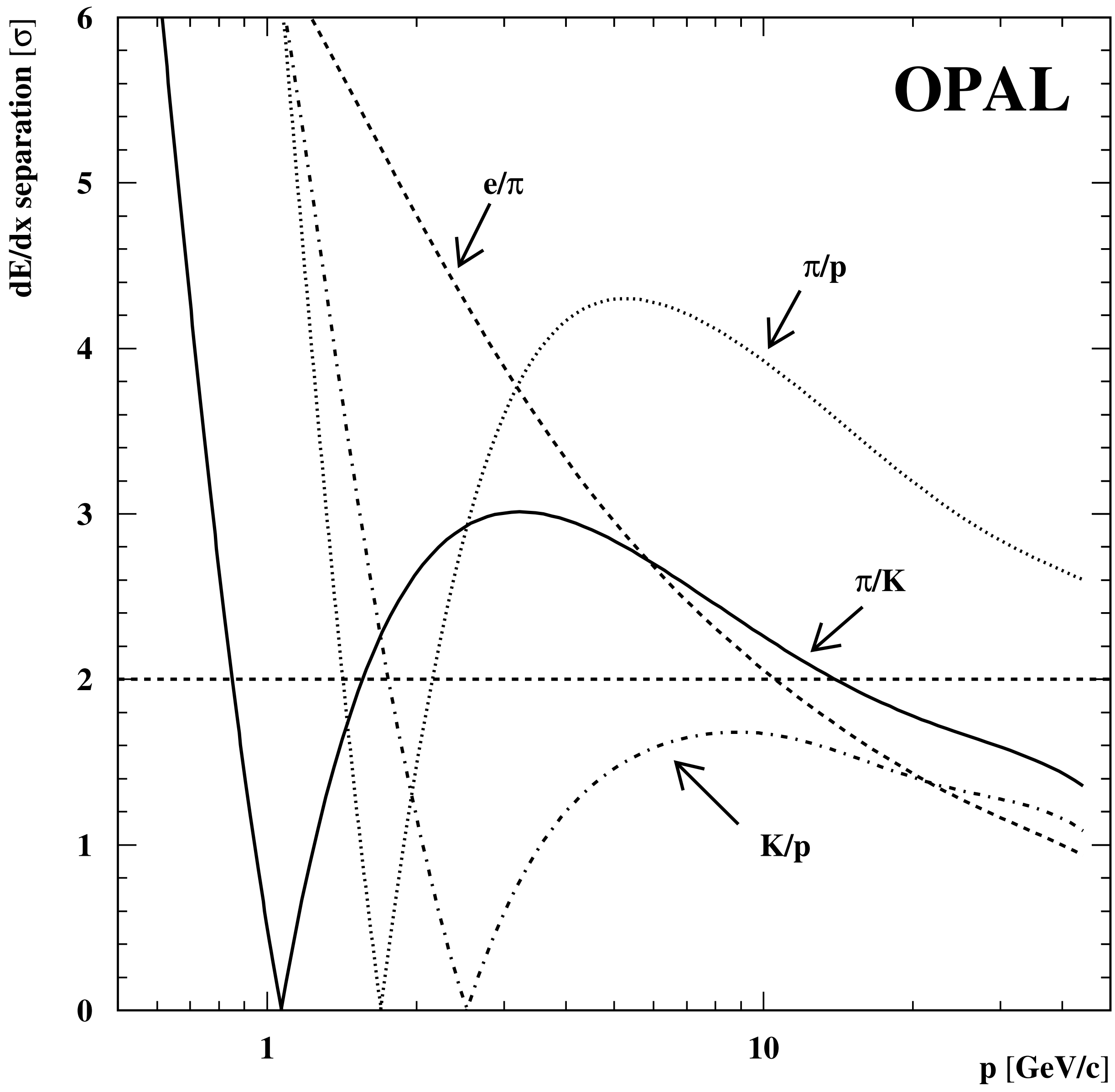

Figure 1: Separation power of the dE/dx measurement for the different particle species as a function of particle momentum. The curves given are for electron/pion, pion/kaon, pion/proton, and kaon/proton separation.

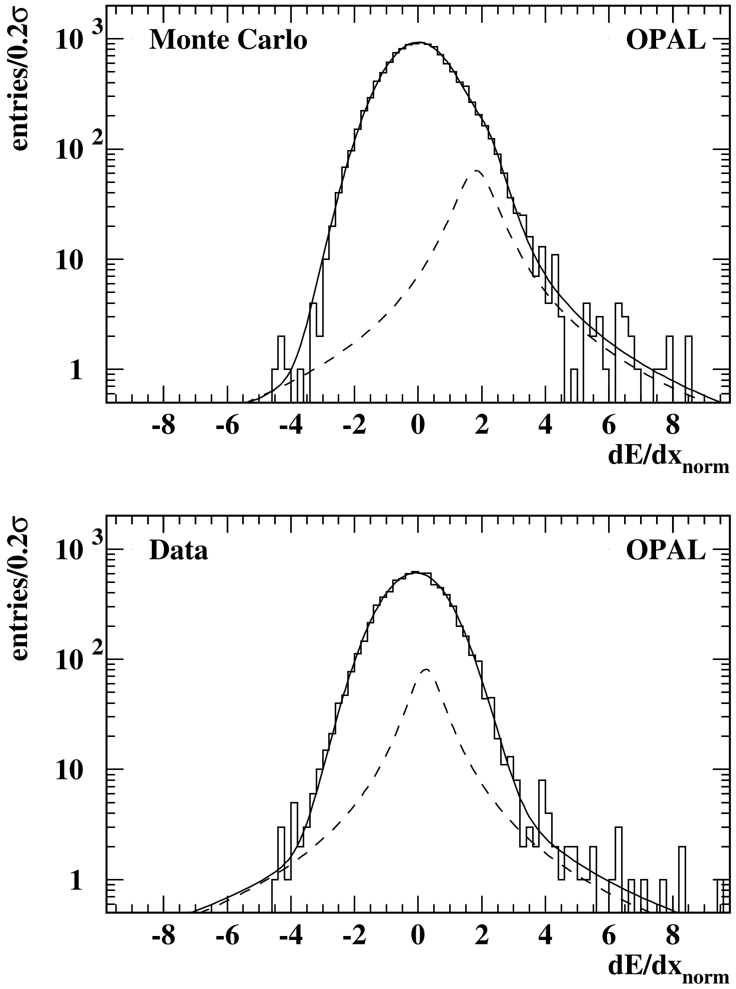

Figure 2: Normalized $\mathrm{d}E/\mathrm{d}x$ distributions for $\pi^{\pm}$ from K^0_S decays in Monte Carlo and experimental data in the momentum interval $3.669\,\mathrm{GeV}/c < p < 3.857\,\mathrm{GeV}/c$. The solid lines are fits of equation (4). The dashed lines indicate the Breit-Wigner term of equation (4).

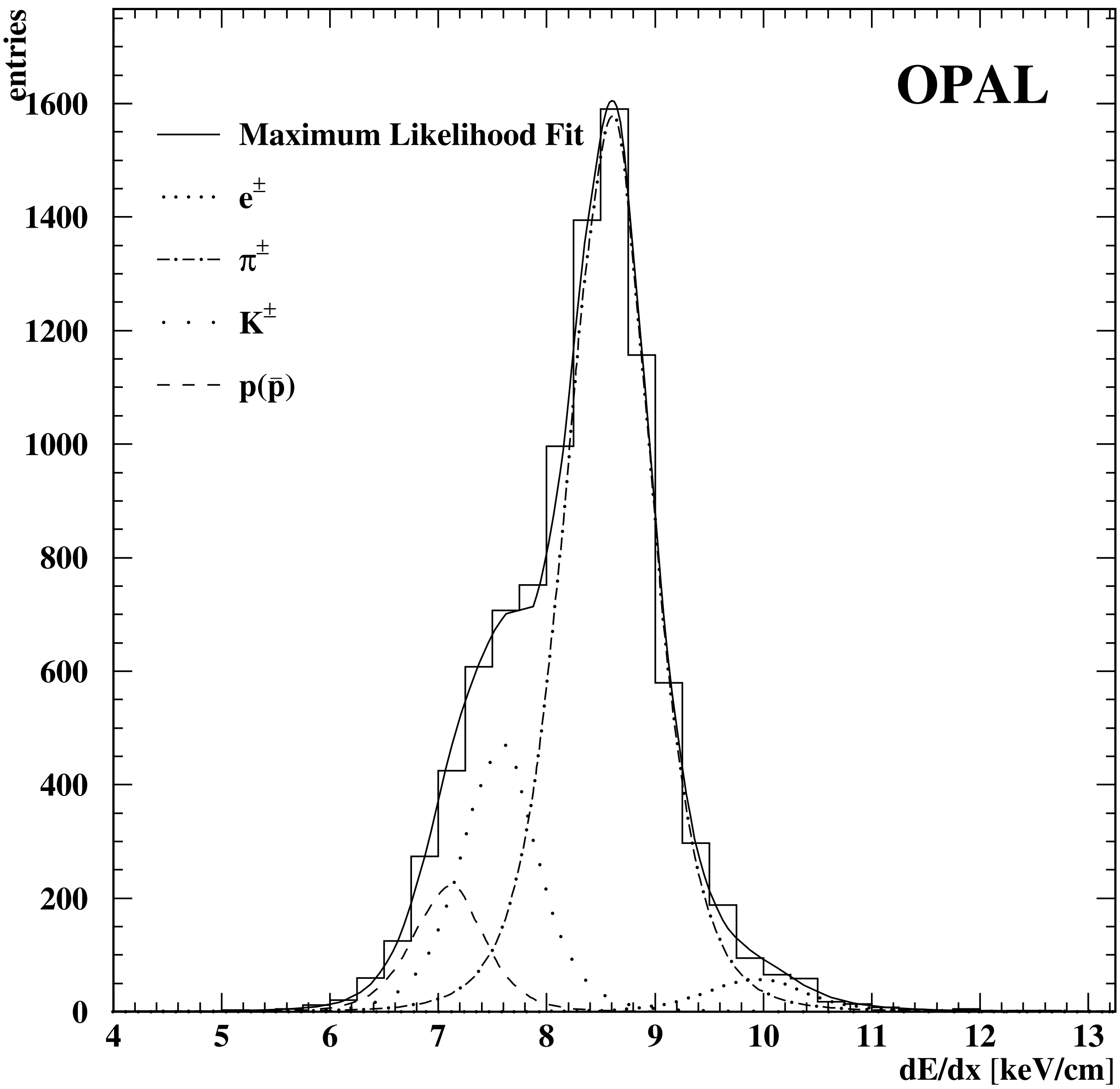

Figure 3: $\mathrm{d}E/\mathrm{d}x$ distribution in the momentum interval $3.669\,\mathrm{GeV}/c < p < 3.857\,\mathrm{GeV}/c$. Superimposed are the results of the maximum likelihood fit and the probability distributions for the individual particle species.

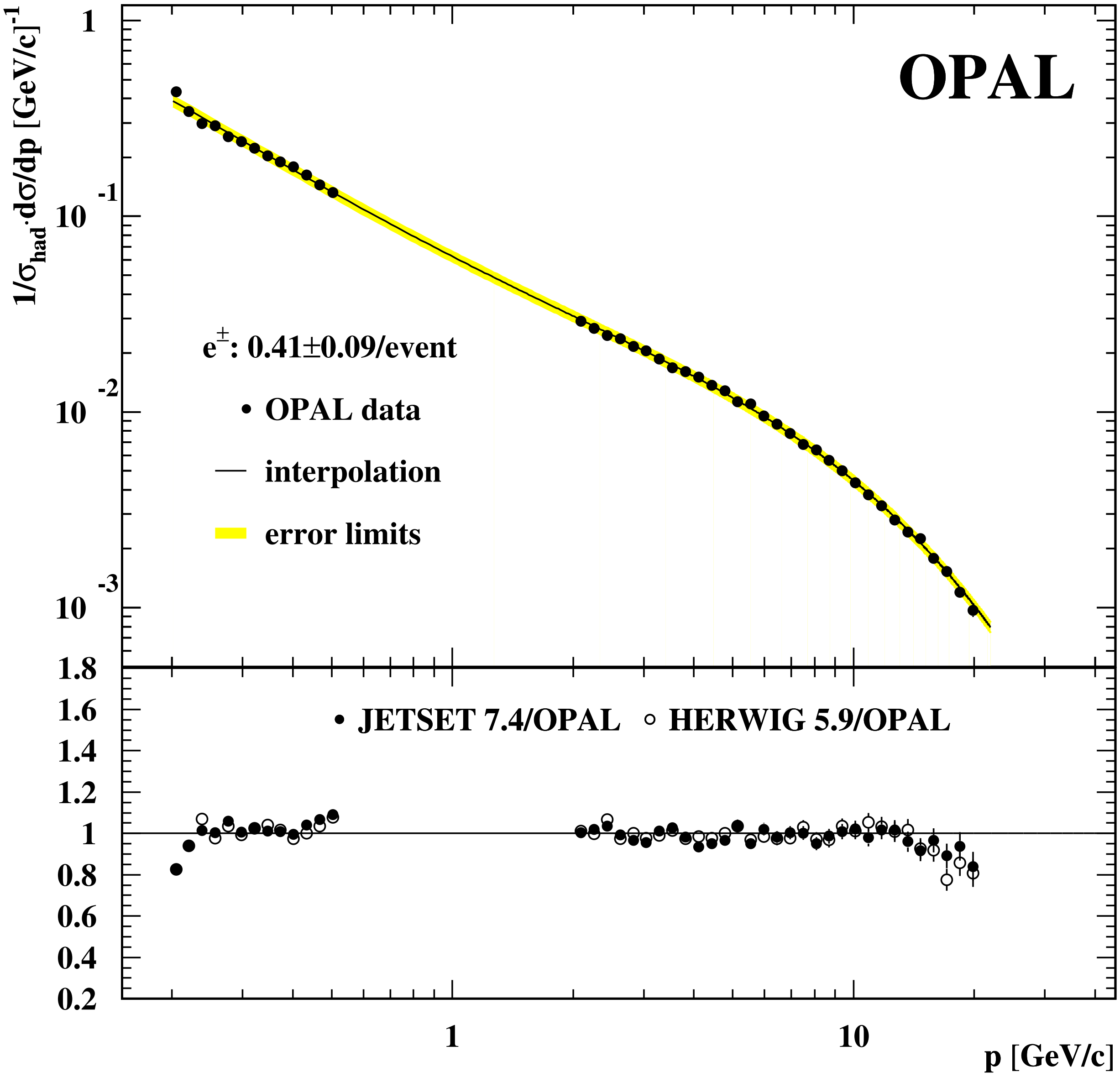

Figure 4: Differential cross-section for electrons as a function of the momentum p. The shaded band indicates the upper and lower limit of the systematic errors (see text). The bottom part of the figure shows the ratios of the JETSET 7.4 and HERWIG 5.9 Monte Carlo predictions to the measurements.

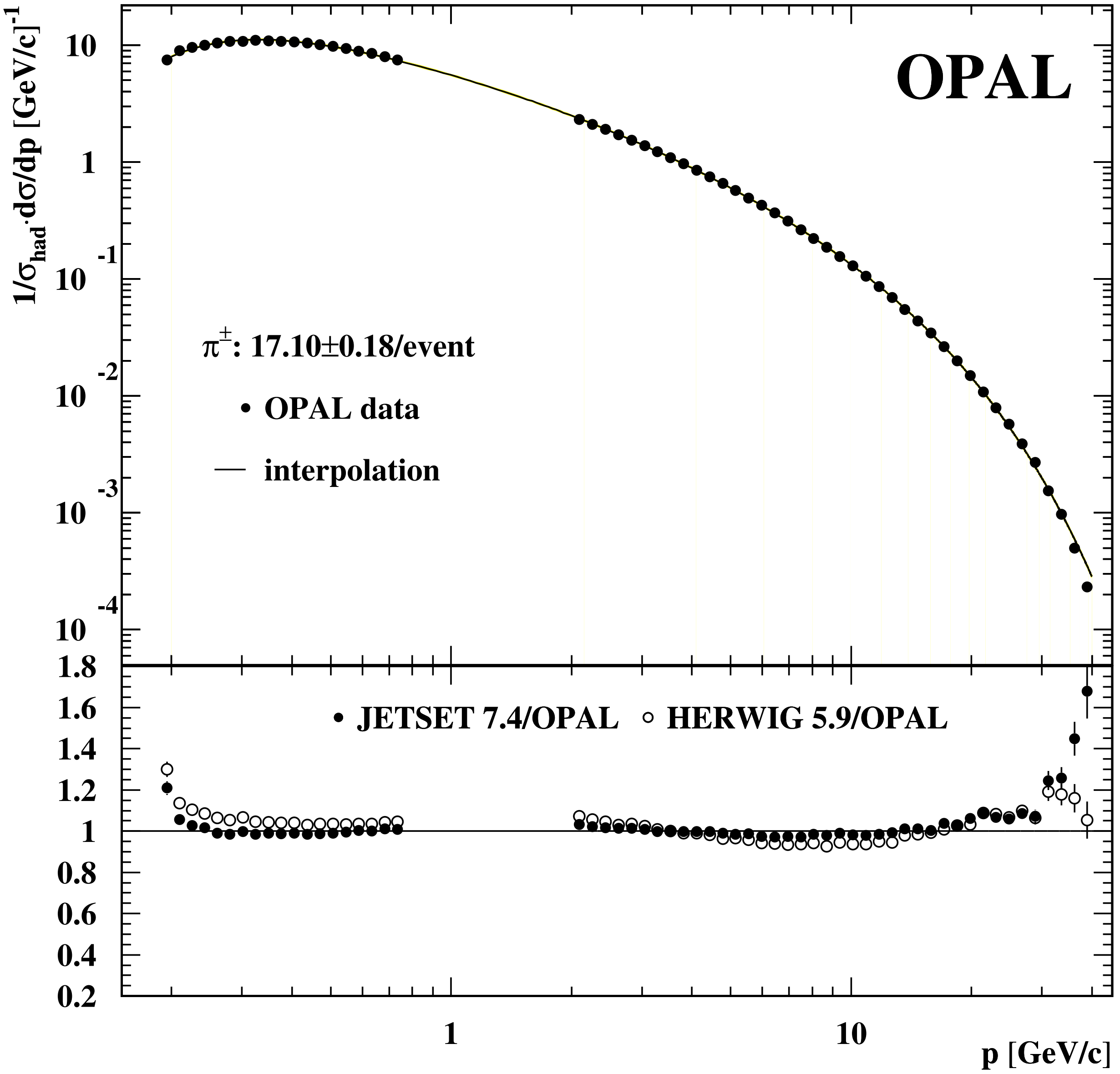

Figure 5: Differential cross section for pions as a function of momentum p. The shaded band of the error limits (see text) is not shown here because it is indistinguishable from the interpolation function. The bottom part of the figure shows the ratios of the JETSET 7.4 and HERWIG 5.9 Monte Carlo predictions to the measurements. The model predictions have been scaled by the weighted average over the bins of the ratios of data to model.

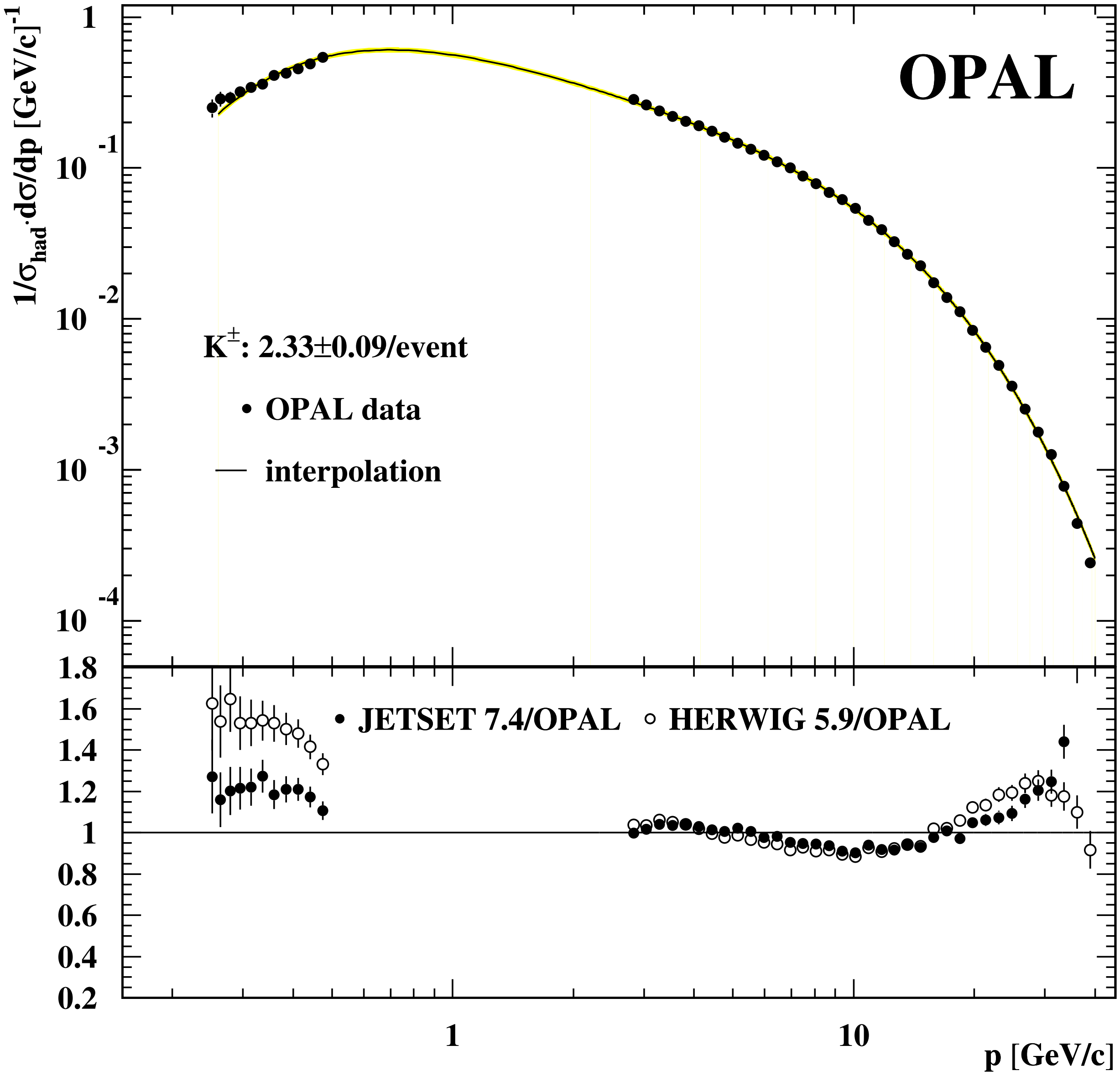

Figure 6: Differential cross section for kaons as a function of momentum p. The shaded band indicating the upper and lower limit of the systematic errors (see text) is not shown because it is indistinguishable from the interpolation function. The bottom part of the figure shows the ratios of the JETSET 7.4 and HERWIG 5.9 Monte Carlo predictions to the measurements. The model predictions have been scaled by the weighted average over the bins of the ratios of data to model.

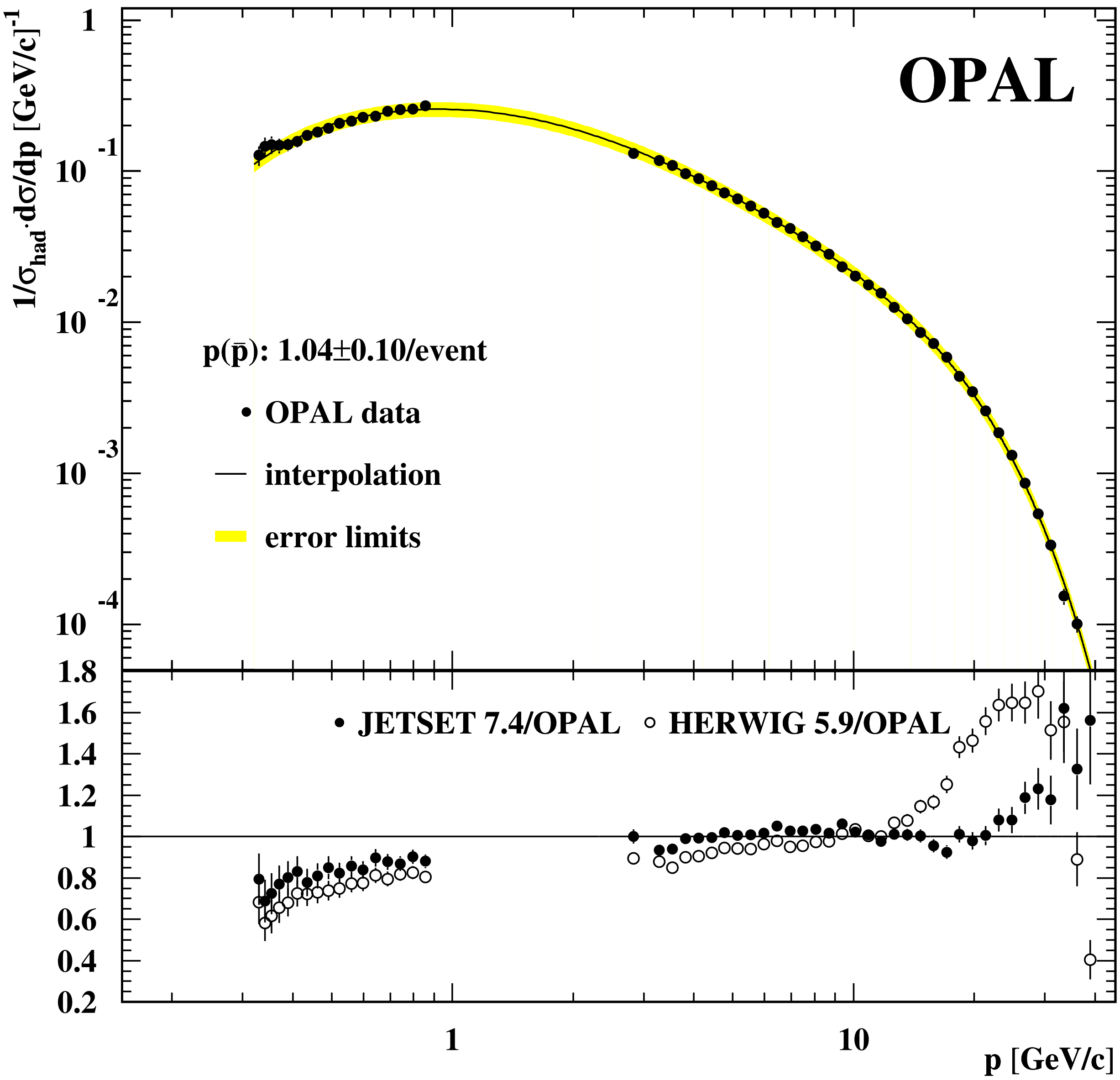

Figure 7: Differential cross section for protons as a function of momentum p. The shaded band indicates the upper and lower limit of the systematic errors (see text). The bottom part of the figure shows the ratios of the JETSET 7.4 and HERWIG 5.9 Monte Carlo predictions to the measurements. The model predictions have been scaled by the weighted average over the bins of the ratios of data to model.

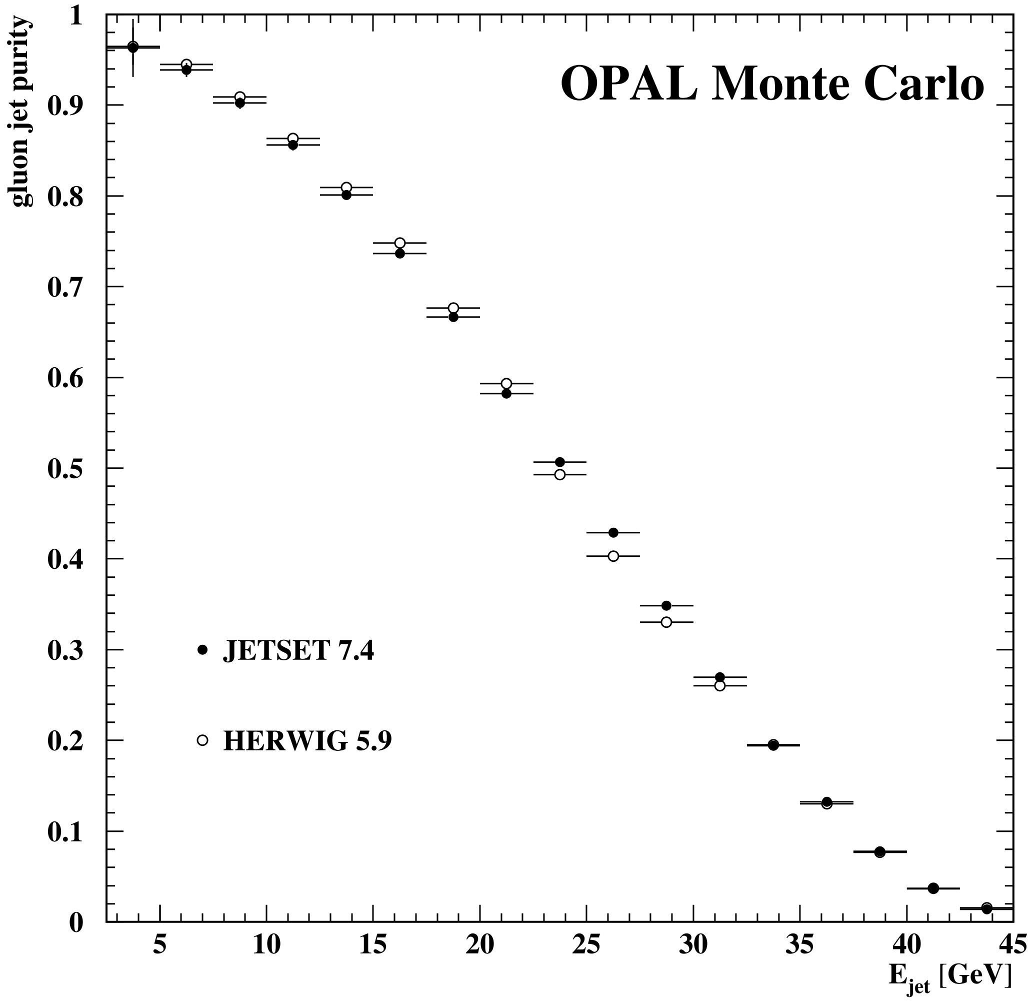

Figure 8: Gluon jet purity as a function of the jet energy.

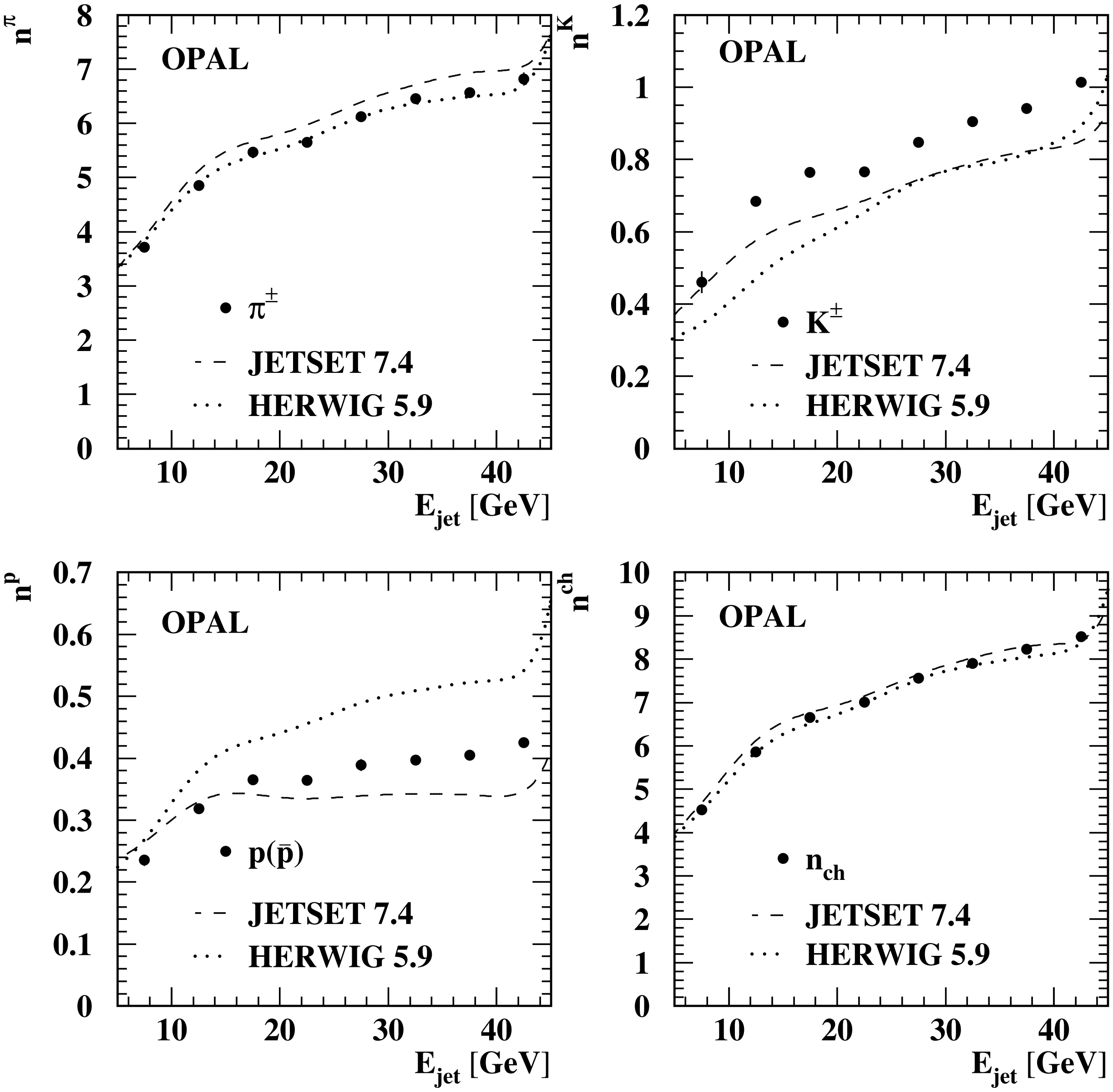

Figure 9: Charged particle rates n^{π}, $n^{\rm K}$, $n^{\rm p}$ and charged multiplicity $n^{\rm ch}$ as a function of the jet energy. The errors shown are the statistical and uncorrelated systematic errors added in quadrature. The dashed lines are the predictions of the JETSET 7.4 model and the dotted lines are the predictions of the HERWIG 5.9 model.

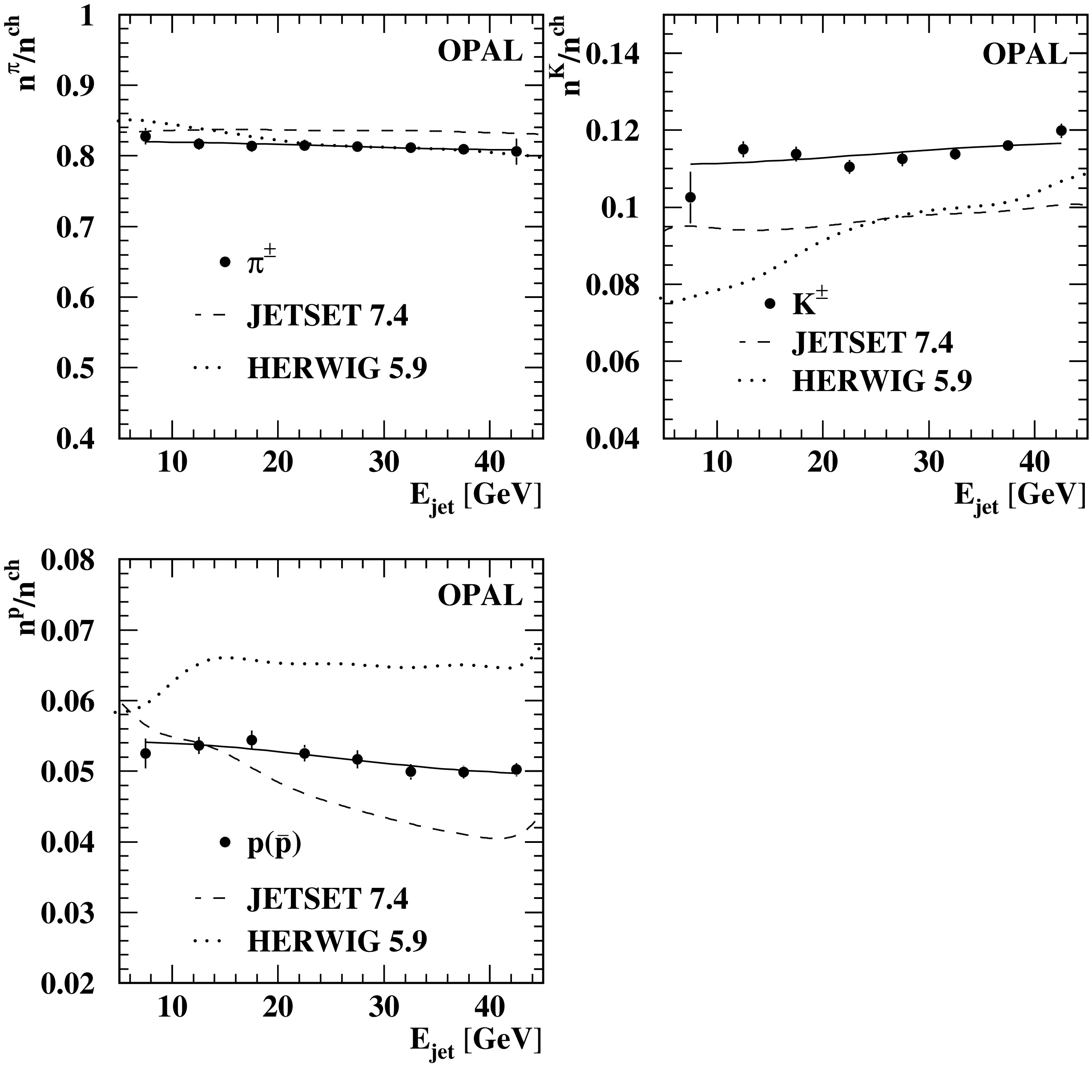

Figure 10: Normalized charged particle rates n^i/n^{ch} as a function of the jet energy. The errors shown are the statistical and uncorrelated systematic errors added in quadrature. The solid lines are the fits of equation (6). The dashed lines are the predictions of the JETSET 7.4 model and the dotted lines are the predictions of the HERWIG 5.9 model.